Electronic Supplementary Information

Microwave-assisted functionalization of carbon nanohorns with oligothiophenes units with SERS activity

Daniel Iglesias,[a] Javier Guerra,[b] María Isabel Lucío,[c] Rafael C. González-Cano,[d] Juan T. López Navarrete,[d] M. Carmen Ruiz Delgado,[d] Ester Vázquez[e,f], M. Antonia Herrero[e,f]

a. Université de Strasbourg, CNRS, ISIS, 8 allée Gaspard Monge, 67000 Strasbourg, France.
b. Facultad de Ciencias, Universidad de Valladolid, 47011, Valladolid, Spain
c. Instituto Interuniversitario de Investigación de Reconocimiento Molecular y Desarrollo Tecnológico (IDM), Universitat Politècnica de València, Universitat de València, Camino de Vera s/n, 46022 Valencia, Spain.
d. Department of Physical Chemistry, University of Málaga, Campus de Teatinos s/n, Málaga 29071, Spain.
e. Facultad de Ciencias y Tecnologías Químicas, Universidad de Castilla-La Mancha (UCLM), 13071 Ciudad Real, Spain
f. Instituto Regional de Investigacion Científica Aplicada (IRICA), 13071 Ciudad Real, Spain

Table of contents

1. General Information

1.1.Materials

All chemicals and solvents were purchased from commercial suppliers and used without prior purification. Carbon nanohorns were purchased at Carbonium s.r.l. Single-walled carbon nanotubes were purchased from Carbon Nanotechnologies Inc. (HiPco® Single-Wall CarbonNanotubes, lot number R0513).

1.2.Methods

Thermogravimetric analyses were recorded with a thermogravimetric analyzer Q50 (TA Instruments). The analyses were performed under N_2 from 100°C to 900 °C by using a 10 °C min^{-1} ramp.

Raman spectroscopy was carried out in a Renishaw InVia microspectrometer equipped with a high-resolution grating (2400 grooves cm^{-1}), a confocal microscope and a 2D-CCD camera. All samples were focused with a ×100 lens and were excited with a red laser (633 nm). The power of the laser was kept under 0.25 mW to avoid damaging the sample. All the reported spectra correspond to the average of several data points to assure the homogeneity of the samples.

UV-Vis spectroscopy was performed on a Varian Cary 5000 spectrophotometer using 1 cm path-length quartz cuvettes. Carbon nanostructures (1 mg) were bath-ultrasonicated in $CHCl_3$ (100 ml) for 15 min before the acquisition.

Transmission electron microscopy images were collected on a Philips EM 208 microscope operating at 100 kV. The dispersion of the sample was drop-casted on top of carbon film TEM grids that were dried under vacuum before the analysis.

Density Functional theory (DFT) calculations were carried out by means of the Gaussian 09 program.[1] The M06-2X[2] functional with the standard 6-31G** basis set[3,4] were used for the geometry optimizations. The M06-2X functional was chosen because of its ability to describe π–π interactions and estimate the energies of weak intermolecular interactions.[5,6] All geometrical

parameters were allowed to vary independently apart from planarity of the rings and no symmetry constraints were imposed during the optimization process. On the resulting ground-state optimized geometries, harmonic vibrational frequencies and Raman intensities were calculated analytically at M06-2X/3-21* level. The more widely used B3LYP[7] was also used to evaluate the ground-state geometries and Raman frequencies of carbon nanohorns. In general, the results (*i.e.*, Raman frequencies and intensities) were very similar when compared to those obtained at the B3LYP level. Molecular orbitals were rendered from geometry optimizations outputs with Chimera 1.11.2 software.[8]

We started with a CNH structure consisting of 360 carbon atoms terminated by 24 hydrogen atoms proposed by Dos Santos *et al.*[9] This conformation where the pentagons set apart one from another to avoid pentagon-pentagon adjacencies was the most stable conformation found among several topologies with different relative positions of the five pentagons existing in the conical tip. This 360-carbon atom model is however far too large for a systematic DFT study, therefore we restricted our model by removing the three outmost strips of 6-membered rings from this previous model resulting in a model containing 214 carbon atoms, terminated by 20 hydrogen atoms. Our nanohorn model has a shape with measured cone angles of 19.2° with a diameter of ≈13.2 Å at the wide end. In postulating how terthiophene interacts with the carbon nanohorn, four different conformations were examined considering two different binding sites of the CNH surface (i.e., close to the cone tip and on the lateral face of the nanohorns) and two different orientations of the terthiophene relative to the CNH surface (named as *1* and *2*). The binding energy is calculated for each configuration as the difference between the calculated energy of the functionalized *f*-CNH 3 system minus the sum of the calculated energies for *p*-CNH and the terthiophene-$CHNHCH_2$ fragment (BE = E [*f*-CNH 1]-E[*p*-CNH]-E[terthiophene-$CHNHCH_2$]). The models for *f*-CNH 1 and *f*-CNH 2 were built taken *f*-CNH 3 as a reference model in tip2 configuration.

In order to compare the CNH behaviour with other carbon nanostructure, structure construction of the zig-zag (12,0) Single-Walled Carbon Nanotube (SWCNT) was performed with NanoCap 1.0.1[10] software, by the use of the empirical carbon potential through the use of the Large Atomic/Molecular Massively Parallel Simulator (LAMMPS).[10] We employed a $C_{198}H_{12}$ cluster model, to represent an one-capped CNT. The boundaries of the nanotube were saturated with

hydrogen atoms, which is a typical procedure for covalent materials. Substitution pattern of the terthiophene on the CNT was built following two non-equivalent placings on the CNT cap (tip1 and tip2) and wall (lateral1 and lateral2), analogously to *f*-CNH 3.

2. Experimental protocols

2.1.Functionalization of carbon nanohorns

The functionalization was carried out following a previously reported protocol.[11] In a microwave quartz vessel, 25 mg of pristine CNHs, glycine (4) (50 mg, 0.66 mmol) and the corresponding aldehyde (1-3) (0.66 mmol) were ultrasonicated in CH_2Cl_2 (10 mL) for 5 min. After ultrasonication, the solvent was removed using a nitrogen stream. The vessel was sealed and introduced in a monomode microwave reactor. The reaction was irradiated for 45 min. The crude was cooled down to room temperature and then suspended in CH_2Cl_2 (75 mL) and sonicated for 5 min. The resulting dispersion was filtered through a Millipore Membrane (JGWP 0.2 μm). The black solid collected from the filter was purified by cycles of ultrasonication/filtration in different solvents: (i) methanol/HCl (37%) 3/1 (100 mL); (ii) methanol (100 mL); (iii) dimethylformamide (200 mL); and (iv) CH_2Cl_2 (75 mL). The product was eventually dried under vacuum affording the desired material as black solids (*f*-CNH 1 (26 mg), *f*-CNH 2 (22 mg) and *f*-CNH 3 (27 mg)). Analogously, *f*-CNH 3 was prepared using sarcosine instead of glycine.

2.2.Calculation of the degree of functionalization

The degree of functionalization is calculated using the data extracted from the thermograms. Below, the calculation of the degree of functionalization for *f*-CNH 3 is shown as an example.

1. From the thermogram, the difference of weight loss between p-CNH and *f*-CNH 3 at 550 °C is attributed to the functionalization:

$$99.7\ \% - 86.7\% = 13\ \%\ of\ functional\ molecule$$

2. Therefore,

$$\frac{0.13\ g\ of\ functional\ molecule}{1\ g\ of\ f-CNH\ 3}$$

3. Considering the molecular weight of the grafted function, 290 g/mol for *f*-CNH 3, the number of micromoles of functional groups per gram of CNH can be calculated:

$$\frac{0.13\ g\ of\ functional\ molecule}{1\ g\ of\ f-CNH\ 3} \times \frac{1\ mol\ of\ functional\ molecule}{290\ g\ functional\ molecule} \times \frac{10^6 \mu mol}{1\ mol} = 448\ \mu mol/g$$

2.3.Synthesis of control-CNH

The functionalization was carried out following a previously reported protocol.[12] Pristine CNHs (10 mg) and 2,2':5',2"-terthiophene-5-carboxaldehyde 3 (40 mg) were ultrasonicated in $CHCl_3$ (10 mL) for 15 min. The resulting dispersion was stirred for 48 h at room temperature. After that, the crude was filtered through a Millipore Membrane (JGWP 0.2 μm). The black solid collected from the filter was purified by cycles of ultrasonication/filtration in different solvents (*o*-dichlorobenzene (200 mL), $CHCl_3$ (100 mL), CH_2Cl_2 (100 mL) and diethyl ether (50 mL)). Afterwards the product was dried under vacuum affording 8 mg of composite.

2.4.Functionalization of carbon nanotubes

f-CNT 3 (21 mg) was prepared following the same procedure applied for *f*-CNH 3 but using CNTs instead of CNHs.

3. Supplementary figures

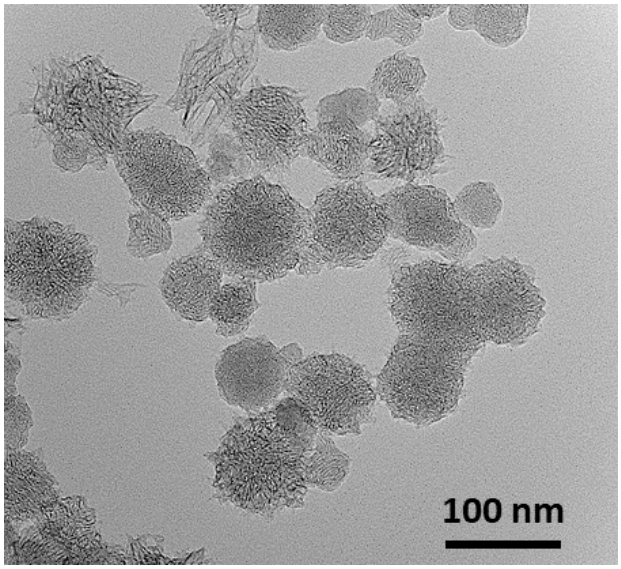

Figure S 1. Transmission microscopy image of *p*-CNH.

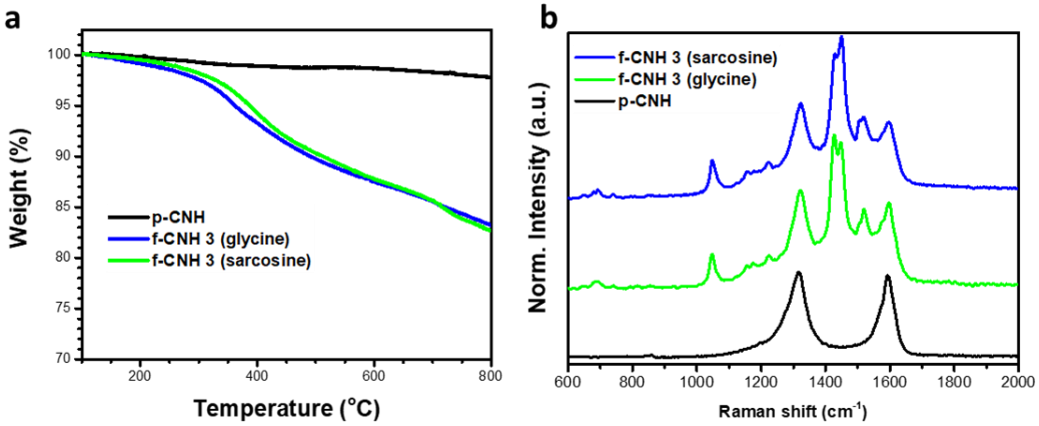

Figure S 2. (a) TGA and (b) Raman characterization of *p*-CNH and *f*-CNH 3 with glycine or sarcosine. The data show that the functionalization and Raman enhancement are analogous in both cases.

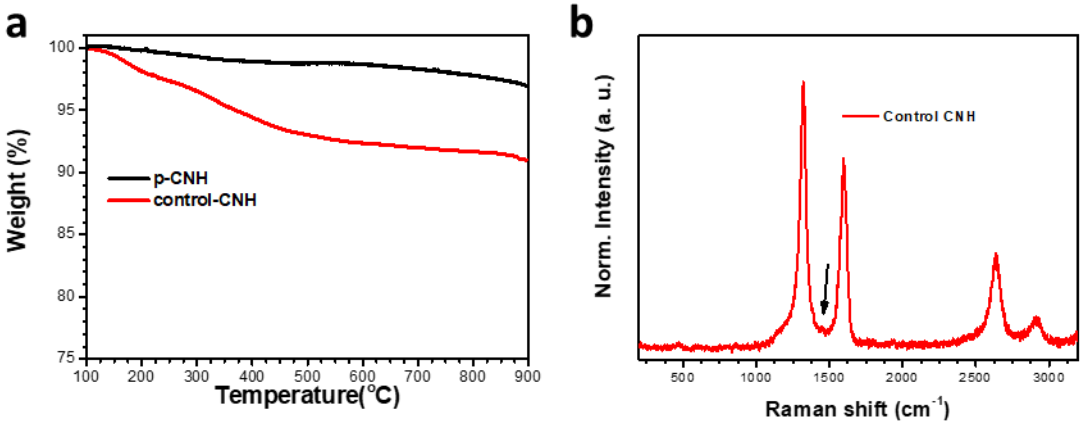

Figure S 3. (a) TGA of *p*-CNH and control-CNH and (b) Raman characterization of control-CNH. The black arrow in (b) indicates the trace of the signal of aldehyde 3.

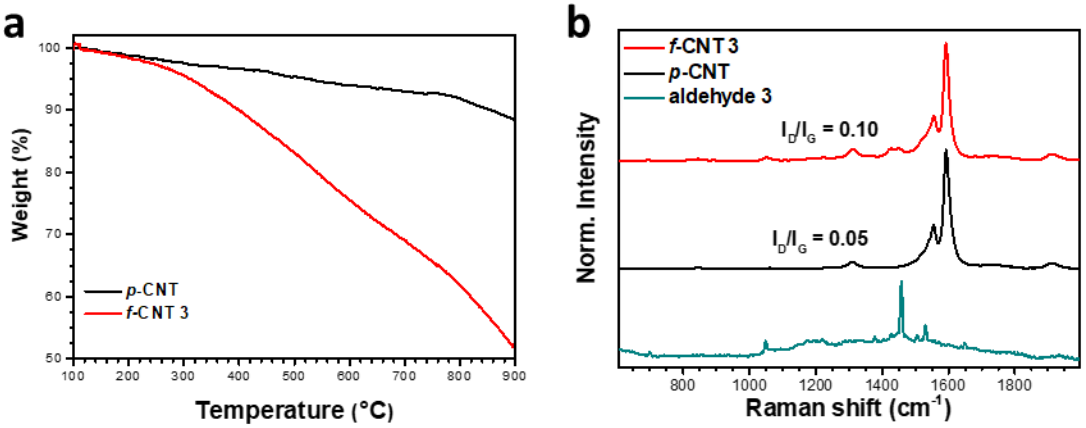

Figure S 4. (a) TGA and (b) Raman characterization of *f*-CNT 3. The Raman of aldehyde 3 was added for the sake of comparison.

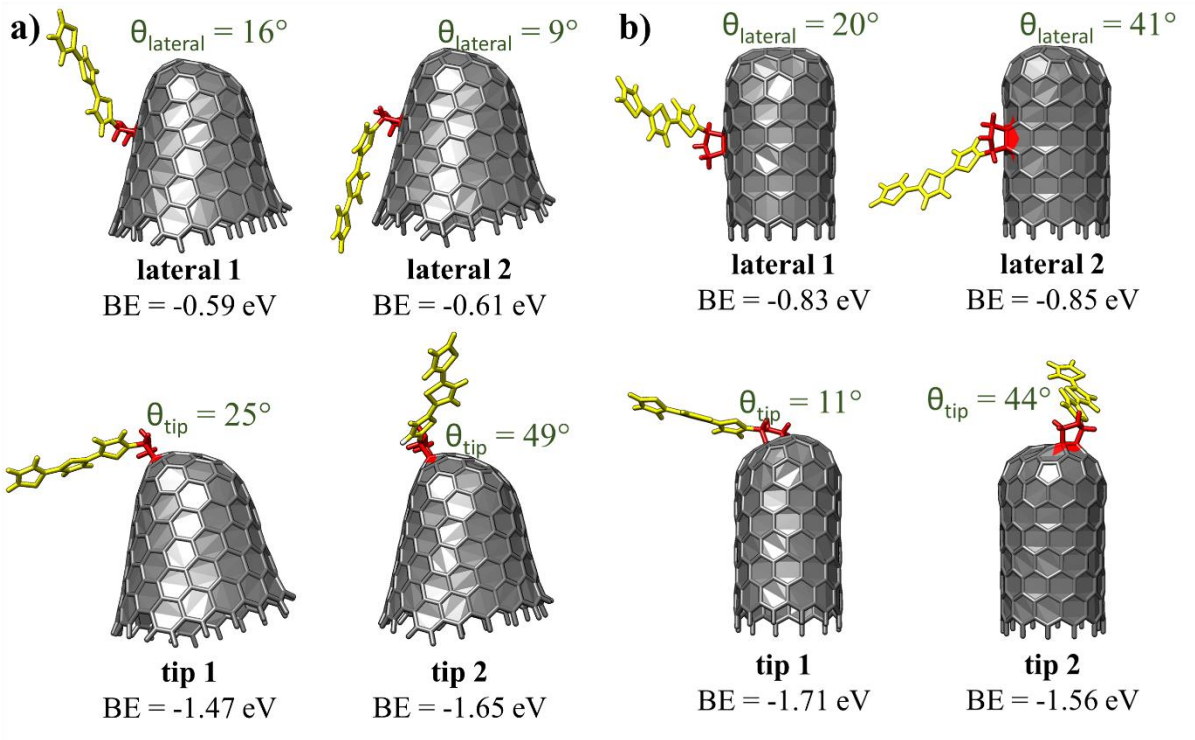

Figure S 5. DFT-optimized geometries of the *f*-CNH 3 (a) and *f*-CNT 3 (b) models in four different configurations calculated at the M06-2X/6-31G** level. Binding energy (BE) values and the angles between the planes formed by the terthienyl unit and the conical tip (Θ_{tip}) and by the terthienyl unit and the lateral surface ($\Theta_{lateral}$) are also shown.

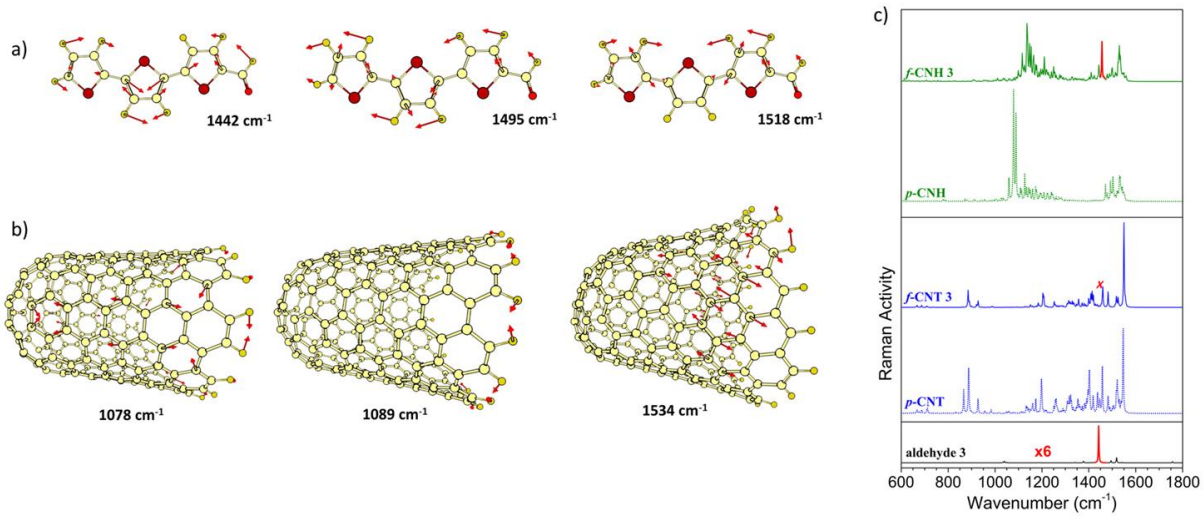

Figure S 6. M06-2X/3-21G* vibrational eigenvectors associated with the most outstanding Raman features of (a) aldehyde 3 and (b) *p*-CNH. (c)Theoretical Raman spectra of aldehyde 3, *p*-CNH, *p*-CNT and functionalized *f*-CNH 3, *f*-CNT 3 in tip 2 configuration.

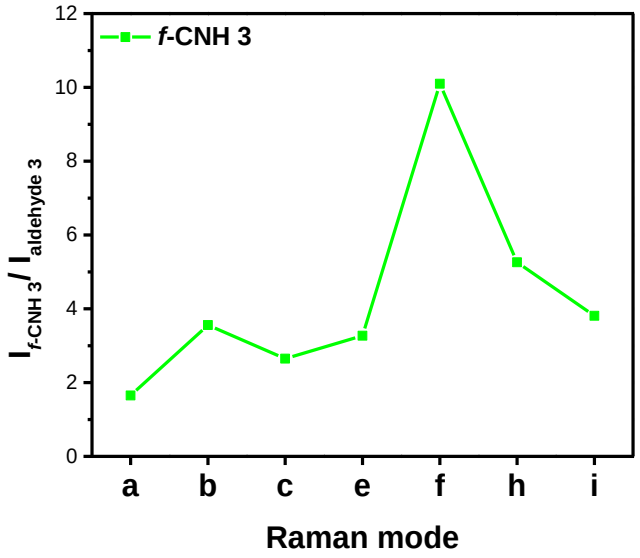

Figure S 7. Relative Raman Intensity of the aldehyde 3 deposited on the SiO_2/Si compared to the derivative *f*-CNH 3. Note that the reported Raman enhancement is underestimated as the amount of terthienyl units in *f*-CNH 3 is smaller than in pure aldehyde 3.

Table S 1. Raman shifts of the characteristic peaks found in the spectra and the corresponding calculated wavelengths.

band	aldehyde 3 exp.	aldehyde 3 theo.	*f*-CNH 3[a] theo.	*f*-CNH 3 exp.	DESCRIPTION	SYMBOL
a	700	691	688	692	CS in-plane bending	δ (CS)
b	1048	1039	1046	1048	Out-of-phase ring C-H in-plane bending	δ_a (CH)
c	1152	1185	1189	1156	C-C in-plane bending	δ (CC)
e	1219	1236	1203	1223	In-phase ring C-H in-plane bending	δ_s (CH)
f	1457	1442	1456	1450	In-phase C=C stretching	υ_s (C=C)
h	1506	1495	1500	1506	Out-of-phase C=C stretching	υ_a (C=C)
i	1531	1518	1529	1520	Out-of-phase C=C stretching	υ_a (C=C)

[a] Calculated in tip 2 *configuration*.

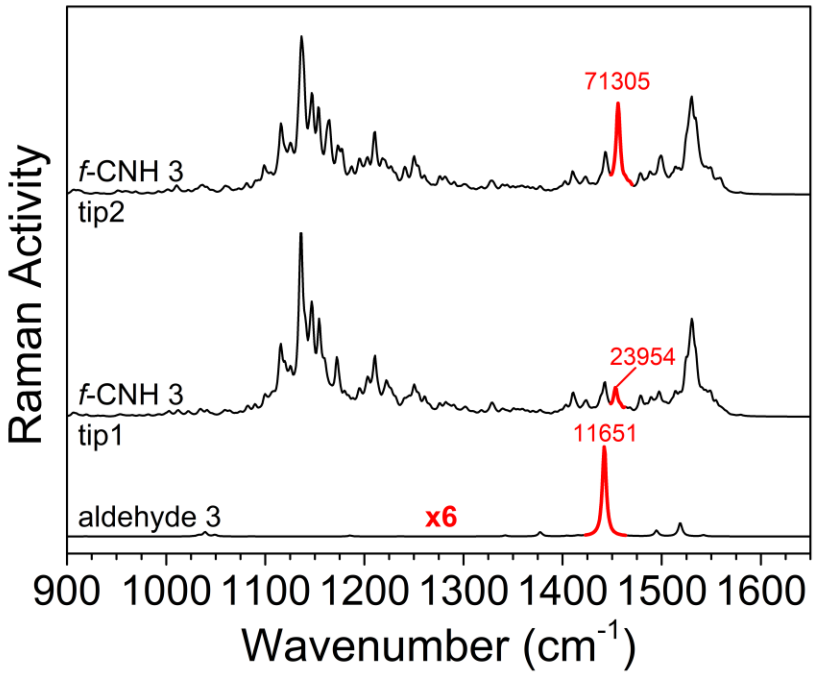

Figure S 8. Theoretical Raman spectra of functionalized *f*-CNH 3 in tip 1 and tip 2 configurations (see Figure S3). The bands associated with the C=C/C-C stretching mode localized on the terthiophene group are denoted in red; the calculated Raman scattering activity values (in A^4/AMU) associated to this mode are also shown.

Table S 2. DFT calculated bond-length alternation (BLA) values and dihedral angles for the aldehyde) and functionalized *f*-CNH 3. The values in parentheses correspond to a terthiophene linked to a pyrrolidine unit.

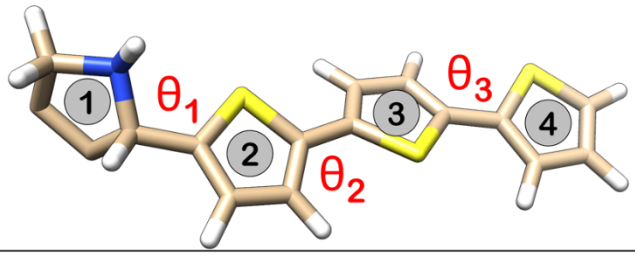

BLA values (Å)

rings	terthiophene	*f*-CNH 3			
		tip1	*tip2*	*lateral1*	*lateral2*
1	(0.005)	-0.014	-0.018	0.027	0.019
2	0.038 (0.057)	0.053	0.054	0.052	0.052
3	0.046 (0.049)	0.048	0.048	0.048	0.045
4	0.057 (0.057)	0.057	0.057	0.057	0.059

Dihedral angles (°)

θ	terthiophene	*f*-CNH 3			
		tip1	*tip2*	*lateral1*	*lateral2*
θ_1	1 (92)	114	-91	-86	84
θ_2	163 (157)	161	157	163	165
θ_3	158 (157)	158	157	159	171

Table S 3. DFT calculated bond-length alternation (BLA) values and dihedral angles for the aldehyde 3 and functionalized *f*-CNT 3. The values in parentheses correspond to a terthiophene linked to a pyrrolidine unit.

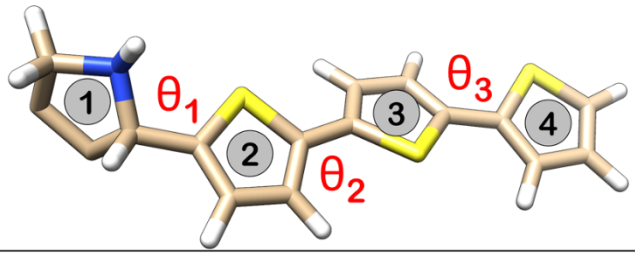

BLA values (Å)

rings	terthiophene	*f*-CNT 3			
		tip1	*tip2*	*lateral1*	*lateral2*
1	(0.005)	0.036	0.033	0.003	0.002
2	0.038 (0.057)	0.054	0.056	0.053	0.052
3	0.046 (0.049)	0.049	0.048	0.048	0.048
4	0.057 (0.057)	0.058	0.057	0.057	0.057

Dihedral angles (°)

θ	terthiophene	*f*-CNT 3			
		tip1	*tip2*	*lateral1*	*lateral2*
θ_1	1 (92)	87	107	119	45
θ_2	163 (157)	158	165	160	163
θ_3	158 (157)	158	158	159	158

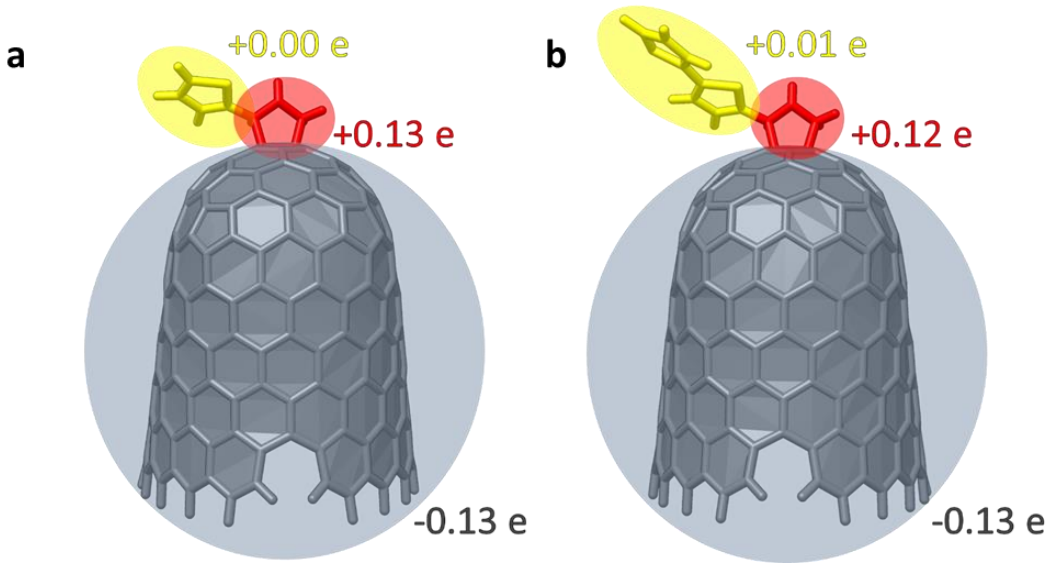

Figure S 9. Mülliken atomic charges on different molecular domains for *f*-CNH 1 and *f*-CNH 2 in tip 2 configuration.

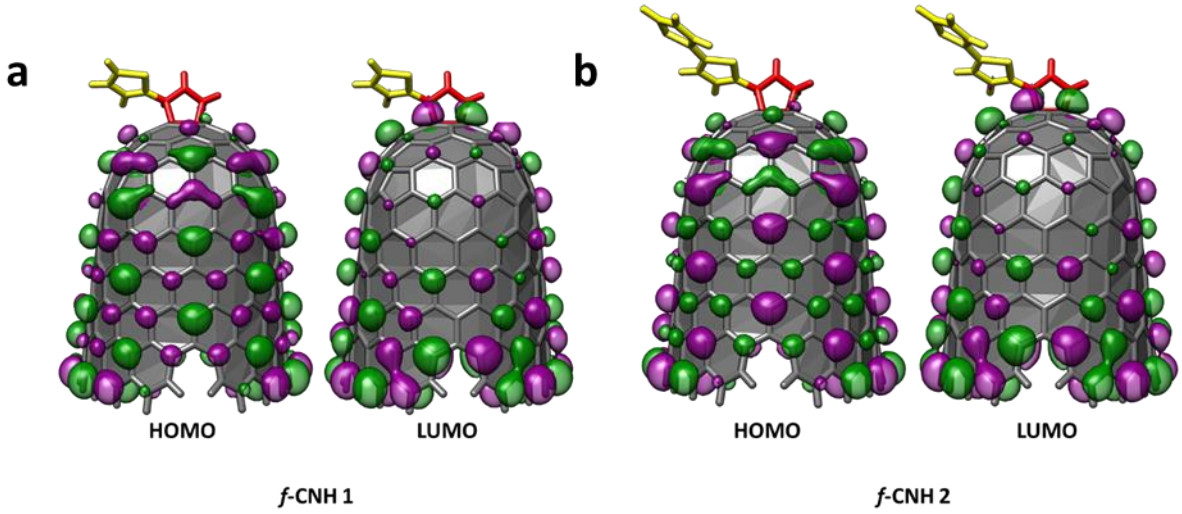

Figure S 10. Topologies of the frontier molecular orbitals of functionalized *f*-CNH 1 and *f*-CNH 2 in tip 2 configuration.

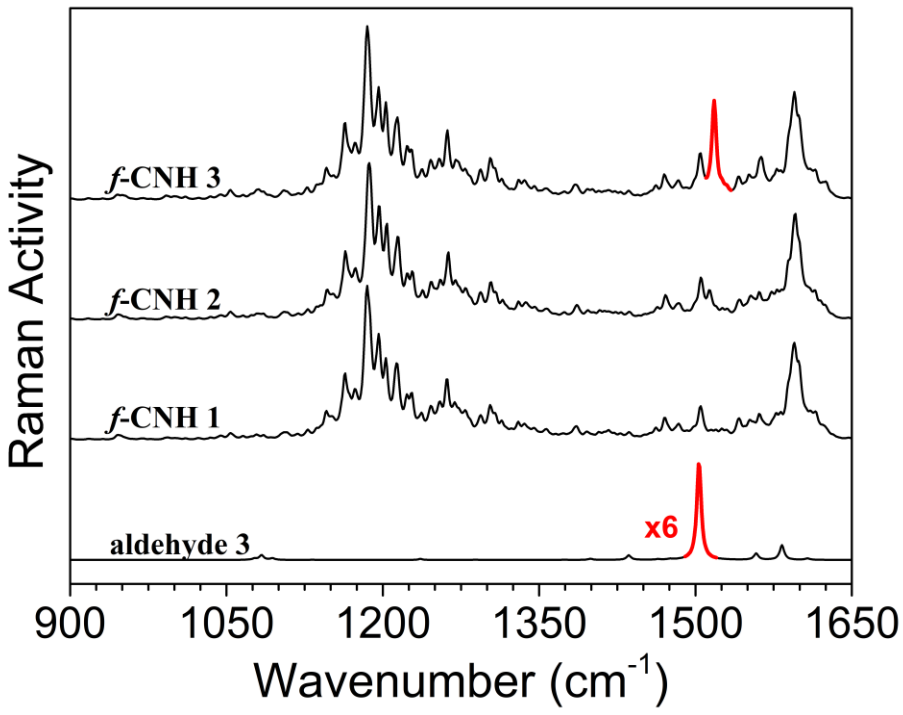

Figure S 11. Theoretical Raman spectra (M06-2X/3-21G*) of functionalized *f*-CNH 1, *f*-CNH 2 and *f*-CNH 3 in tip 2 configuration. The bands associated with the C=C/C-C stretching mode localized on the oligothiophene group are denoted in red.

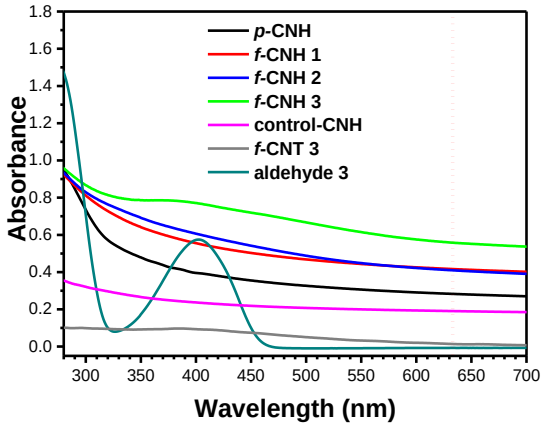

Figure S 12. UV-Vis spectra of the most relevant materials in $CHCl_3$ (0.01 mg/ml). The dotted line indicated the position of the red laser (633 nm) used for the Raman analysis.

4. References

1 M.J.Frisch,G. W. Trucks, H. B. Schlegel, G. E. Scuseria, M. A. Robb, J. R. Cheeseman, G. Scalmani, V. Barone, G. A. Petersson, H. Nakatsuji, X. Li, M Caricato, A. V. Marenich, J. Bloino, B. G. Janesko, R. Gomperts, B. Mennucci, H. P. Hratchian, J. V. Ortiz, J. L. Izmaylov, J. L. Sonnenberg, Williams, F. Ding, F. Lipparini, F. Egidi, J. Goings, B. Peng, A. Petrone, T. Henderson, D. Ranasinghe, V. G. Zakrzewski, J. Gao, N. Rega, G. Zheng, W.Liang, M. Hada, M. Ehara, K. Toyota, R. Fukuda, J. Hasegawa, M. Ishida, T. Nakajima, Y. Honda, O. Kitao, H. Nakai, T.Vreven, K. Throssell, J. A. Jr. Montgomery, J. E. Peralta, F. Ogliaro, M. J. Bearpark, M. J.; Heyd, E. N. Brothers, K. N. Kudin, V. N. Staroverov, T.A. Keith, R. Kobayashi, J. Normand, K. Raghavachari, A. P. Rendell, J. C. Burant, S. S. Iyengar, J. Tomasi, M. Cossi, J. M. Millam, M. Klene, C. Adamo, R. Cammi, J. W. Ochterski, R. L. Martin, K. Morokuma, O. Farkas, J. B. Foresman, D. J. Fox, et al. Gaussian 09, revision C.01; Gaussian Inc.: Wallingford, CT, 2009.

2 Y. Zhao and D. G. Truhlar, *Acc. Chem. Res.*, 2008, **41**, 157–167.

3 W. J. Hehre, D. R and J. A. Pople, *J. Chem. Phys.*, 1972, **56**, 2257.

4 M. M. Francl, W. J. Pietro, W. J. Hehre, J. S. Binkley, M. S. Gordon, D. J. DeFrees and J. A. Pople, *J. Chem. Phys.*, 1982, **77**, 3654−3665.

5 K. E. Riley, M. Pitonak, J. Cerny and P. Hobza, *J. Chem. Theory Comput.*, 2010, **6**, 66–80.

6 I. Badía-Domínguez, A. Pérez-Guardiola, J. C. Sancho-García, J. T. López Navarrete, V. Hernández Jolín, H. Li, D. Sakamaki, S. Seki and M. C. Ruiz Delgado, *ACS Omega*, 2019, **4**, 4761–4769.

7 C. Lee, W. Yang and R. G. Parr, *Phys. Rev. B*, 1988, **37**, 785–789.

8 E. F. Pettersen, T. D. Goddard, C. C. Huang, G. S. Couch, D. M. Greenblatt, E. C. Meng and T. E. Ferrin, *J. Comput. Chem.*, 2004, **25**, 1605–1612.

9 H. F. Dos Santos, L. A. De Souza, W. B. De Almeida and T. Heine, *J. Phys. Chem. C*, 2014, **118**, 24761–24768.

10 M. Robinson and N. A. Marks, *Comput. Phys. Commun.*, 2014, **185**, 2519–2526.

11 N. Rubio, M. A. Herrero, M. Meneghetti, Á. Díaz-Ortiz, M. Schiavon, M. Prato and E. Vázquez, *J. Mater. Chem.*, 2009, **19**, 4407–4413.

12 D. Iglesias, J. Guerra, M. V. Gómez, A. M. Rodríguez, P. Prieto, E. Vázquez and M. A. Herrero, *Chem. - A Eur. J.*, 2016, **22**, 11643–11651.